

Evolution of the Solar Nebula. VIII. Spatial and Temporal Heterogeneity of Short-Lived Radioisotopes and Stable Oxygen Isotopes

Alan P. Boss

Department of Terrestrial Magnetism, Carnegie Institution of Washington, 5241 Broad Branch Road, NW, Washington, DC 20015-1305

boss@dtm.ciw.edu

ABSTRACT

Isotopic abundances of short-lived radionuclides such as ^{26}Al provide the most precise chronometers of events in the early solar system, provided that they were initially homogeneously distributed. On the other hand, the abundances of the three stable isotopes of oxygen in primitive meteorites show a mass-independent fractionation that survived homogenization in the solar nebula. As a result of this and other cosmochemical evidence, the degree of spatial heterogeneity of isotopes in the solar nebula has long been a puzzle. We show here that based on hydrodynamical models of the mixing and transport of isotopic anomalies formed at, or injected onto, the surface of the solar nebula, initially high levels of isotopic spatial heterogeneity are expected to fall to steady state levels ($\sim 10\%$) low enough to validate the use of ^{26}Al for chronometry, but high enough to preserve the evidence for mass-independent fractionation of oxygen isotopes. The solution to this puzzle relies on the mixing being accomplished by the chaotic fluid motions in a marginally gravitationally unstable disk, as seems to be required for the formation of gas giant planets and by the inability of alternative physical processes to drive large-scale mixing and transport in the planet-forming midplane of the solar nebula. Such a disk is also capable of large-scale outward transport of the thermally annealed dust grains found in comets, and of driving the shock fronts that appear to be responsible for much of the thermal processing of the components of primitive meteorites, creating a self-consistent picture of the basic physical processes shaping the early solar nebula.

Subject headings: accretion, accretion disks – hydrodynamics – solar system: formation – planetary systems

1. Introduction

Isotopic evidence has been presented for both homogeneity (e.g., Hsu, Huss & Wasserburg 2003; Guan et al. 2006; Thrane et al. 2006) and heterogeneity (e.g., Simon et al. 1998; Sugiura, Miyazaki, & Yin 2006) of short-lived radioisotopes such as ^{26}Al and ^{60}Fe in the the solar nebula. A high degree of homogeneity is required if the inferred starting ratios of $^{26}\text{Al}/^{27}\text{Al}$ are to be used as precise chronometers for the early solar system (Bizzarro et al. 2004; Halliday 2004; Krot et al. 2005b). The degree of uniformity is equally murky even for stable isotopes such as those of molybdenum, for which both heterogeneity (Yin, Jacobsen & Yamashita 2002; Dauphas, Marty & Reisberg 2002) and homogeneity (Becker & Walker 2003) have been asserted. For samarium and neodymium isotopes, both nebular homogeneity and heterogeneity have been claimed, depending on the stellar nucleosynthesis source (Andreasen & Sharma 2006). The three stable isotopes of oxygen, however, show clear evidence for heterogeneity in primitive meteorites (Clayton 1993). At some level, isotopic heterogeneity must exist. The question then becomes, what level of heterogeneity is to be expected?

The short-lived radioisotope (SLRI) ^{60}Fe must have been synthesized in a supernova (Mostefaoui, Lugmair & Hoppe 2005; Tachibana et al. 2006) and then injected into the presolar cloud (Vanhala & Boss 2000, 2002) or onto the surface of the solar nebula (Desch & Ouellette 2005; Ouellette & Desch 2006). A similar nucleosynthetic event is likely to be the source of the bulk of the solar nebula's ^{26}Al (Limongi & Chieffi 2006; Sahijpal & Soni 2006; however, see Gounelle et al. 2006 for a contrary point of view, and Bizzarro et al. 2006 for evidence that the ^{60}Fe was injected after the ^{26}Al). This injection occurred through narrow Rayleigh-Taylor (R-T) fingers (Vanhala & Boss 2000, 2002) that peppered the disk surface with highly nonuniform doses of SLRIs. The scatter in initial $^{26}\text{Al}/^{27}\text{Al}$ ratios observed in meteoritical components ranging from values of ~ 0 to $\sim 4.5 \times 10^{-5}$ (MacPherson, Davis & Zinner 1995) or even higher values $\sim 7 \times 10^{-5}$ (Young et al. 2005) can be attributed to spatial heterogeneity, temporal heterogeneity (i.e., crystallization at different times, allowing for decay of the SLRIs), or some combination of these two extremes. The fact that these SLRIs were injected into the solar nebula means that immediately following the arrival of each R-T finger, the nebula must have been strongly spatially heterogeneous in terms of the abundances of those isotopes, possibly explaining some of the observed range of $^{26}\text{Al}/^{27}\text{Al}$ ratios.

The wide range in stable oxygen isotope abundances is best explained by self-shielding of molecular CO gas from UV photodissociation at the surface of the solar nebula (Clayton 2002; Lyons & Young 2005; however, see Marcus 2004 for an opposing view) or in the presolar molecular cloud (Yurimoto & Kuramoto 2004) and is not associated with R-T injection

events. Oxygen isotopic anomalies formed at the disk surface most likely could only have been preserved in the outer nebula, however, so the oxygen isotope anomalies may have also originated in a spatially heterogeneous manner. Furthermore, dust-gas fractionation is required in order to affect stable oxygen isotope ratios, and this fractionation process would have been a function of both time and space in the disk.

Besides this evidence for initial spatial heterogeneity, there is also strong evidence for large-scale transport of isotopes and small grains. The presence of both high- and low-temperature phases of silicates in comets requires inward transport of amorphous silicates and outward transport of annealed silicates over large distances (several AU at least) in the solar nebula (Lisse et al. 2006). Isotopic evidence suggests (Bizarro, Baker & Haack 2004) that some Allende chondrules formed with an $^{26}\text{Al}/^{27}\text{Al}$ ratio similar to that of calcium, aluminum-rich inclusions (CAIs). Chondrule formation thus appears to have begun shortly after CAI formation, and to have lasted for ~ 1 to 4 Myr (Amelin et al. 2002). While chondrules are generally believed to have been melted by shock-front heating at asteroidal distances (Iida et al. 2001; Desch & Connolly 2002; Ciesla & Hood 2002), CAIs are generally thought to have formed much closer to the protosun, because of their highly refractory compositions (Wood 2004). On the other hand, recent kinetic evaporation-condensation models (Alexander 2004) have shown that Type A (olivine-rich) chondrules, compact Type A (melilite-rich) CAIs, and compact Type B (pyroxene-rich) CAIs may have formed at asteroidal distances, while Type B (pyroxene-rich) chondrules, Al-rich chondrules, and Type C (anorthite-rich) CAIs may have formed closer to the protosun. Either way, mixing of solids from the inner solar nebula out to asteroidal distances seems to be required in order to assemble chondrules, CAIs, and matrix grains into the chondritic meteorites (Boss & Durisen 2005).

Solids formed close to the protosun may have been carried upward by the protosun's bipolar outflow and lofted onto trajectories that would return them to the surface of the solar nebula at much greater distances (Shu et al. 2001). Alternatively, solids might have been transported outward to asteroidal or cometary distances by mixing processes within the solar nebula, such as generic turbulence or the mixing produced by spiral arms in a marginally gravitationally unstable nebula (Boss 2004a). In the Boss (2004a) models, however, the tracers representing solids tied to the gas were injected into the disk midplane or disk surface in rings or sectors of rings centered on a distance of 9 AU, right in the middle of the most gravitationally active region of the disk. These tracers were then found to be rapidly (in less than 0.001 Myr) transported both inward to 4 AU and outward to 20 AU, the inner and outer boundaries of the computational grid, respectively. The question then arises as to the fate of solids injected onto the surface of the nebula at much greater distances, or residing inside the disk closer to the protostar: can these solids be transported inward, or outward,

respectively, through the chaotic region where the gas giant planets are trying to form?

We present here a new set of three dimensional hydrodynamical models of mixing and transport in the solar nebula that attempts to answer both of these questions about transport and mixing in protoplanetary disks, with an emphasis on the solar nebula. These models are identical to those of Boss (2004a) except that in the new models the color fields representing isotopically distinct parcels of gas or solids are introduced at radial distances of either 6 or 15 AU, instead of at the original 9 AU.

2. Numerical Methods

The disk evolution calculations were performed with a numerical code that uses finite differences to solve the three dimensional equations of hydrodynamics, radiative transfer, and the Poisson equation for the gravitational potential. The code is the same as that used in previous studies of transport in disks (e.g., Boss 2004a, 2006) and has been shown to be second-order-accurate in both space and time through convergence testing (Boss & Myhill 1992). The equations are solved on a spherical coordinate grid. The number of grid points in each spatial direction is: $N_r = 101$, $N_\theta = 23$ in $\pi/2 \geq \theta \geq 0$, and $N_\phi = 256$, for a total of over one million grid points in both hemispheres. The radial grid is uniformly spaced between 4 and 20 AU, with boundary conditions at both the inner and outer edges chosen to absorb radial velocity perturbations. The θ grid is compressed into the midplane to ensure adequate vertical resolution ($\Delta\theta = 0.3^\circ$ at the midplane). The ϕ grid is uniformly spaced, to prevent any bias in the azimuthal direction. The central protostar wobbles in response to the growth of nonaxisymmetry in the disk, thereby rigorously preserving the location of the center of mass of the star and disk system. The number of terms in the spherical harmonic expansion for the gravitational potential of the disk is $N_{Ylm} = 32$.

As in Boss (2004a, 2006), the models treat radiative transfer in the diffusion approximation, which should be valid near the disk midplane and throughout most of the disk, because of the high vertical optical depth. Artificial viscosity is not employed. The energy equation is solved explicitly in conservation law form, as are the four other hydrodynamic equations.

3. Turbulent Diffusion

Diffusion of the dust grains carrying the SLRI or oxygen isotope anomalies with respect to the disk gas is handled through a modification of the color equation (e.g., Foster & Boss 1997; Boss 2004a). This modification involves adding in to the right hand side of the color

equation a diffusion term, i.e., second space derivative of the color field, multiplied by an appropriate diffusion coefficient D (e.g., Stevenson 1990). For $D = \text{constant}$, the simplest assumption, the equation of motion for the color field density ρ_c is then

$$\frac{\partial \rho_c}{\partial t} + \nabla \cdot (\rho_c \mathbf{v}) = D \nabla^2 \rho_c,$$

where \mathbf{v} is the disk gas velocity and t is the time. The color equation is solved in the same manner as the five other equations of motion, using finite differences and explicit time differencing.

The models assume (Boss 2004a) that the eddy diffusivity D can be approximated by the eddy viscosity of a classical viscous accretion disk, i.e., $D = \alpha h c_s$, where α = disk turbulent viscosity parameter, h = disk scale height, and c_s = isothermal sound speed at the disk midplane. The same assumption is made by Willacy et al. (2006) in their one dimensional models of chemical effects in the outer regions of protoplanetary disks. For typical nebula values at 5 to 10 AU ($h \approx 1$ AU, $T \approx 100$ K, $c_s \approx 6 \times 10^4$ cm s $^{-1}$), the eddy diffusivity becomes $D = 10^{18} \alpha$ cm 2 s $^{-1}$.

While the color field is subject to eddy diffusivity when $\alpha \neq 0$, the underlying gaseous disk is not – the gaseous disk remains effectively inviscid with an eddy viscosity $\nu = 0$. The eddy diffusivity is thus assumed to be much larger than the eddy viscosity of the gas, i.e., $D \gg \nu$, or $k = D/\nu \gg 1$ (Stevenson 1990). Equivalently, this assumes that the Schmidt number $Sc = \nu/D \approx 0$. For $k = 1$ to 3, turbulent diffusion must work its way upstream against the inward flow onto the protosun, and Stevenson (1990) showed that little upstream mixing occurs in that case. However, Prinn (1990) argued that $k \gg 1$ was likely to occur during early phases of disk evolution when the disk is still accreting material from the infalling cloud envelope, which is the phase of evolution under investigation here. Prinn (1990) pointed out that some turbulent eddies could transport angular momentum inward rather than outward, resulting in a negative contribution to the total disk viscosity, lowering the effective value of ν and resulting in a large value of k . Disks with large k are expected to be able to transport tracers upstream against the inward flow onto the protosun.

Whether $k \gg 1$ or not would depend on the physical mechanisms driving the disk turbulence ν and dust grain diffusion D . For example, in a disk where turbulence is driven by vertical convective motions (as in the present models; see Boss 2004b), Stone et al. (2000) showed that convective cells are sheared by differential rotation to such an extent that the net transport of angular momentum is very small, i.e., $\nu \sim 0$. On the other hand, the magnetorotational instability (MRI) in an ionized disk has been shown to lead to rapid outward angular momentum transport (Stone et al. 2000), so in an MRI-driven disk, one

might expect $k = 1/Sc \sim 1$, as has been found in three dimensional MRI models of mixing in the outer solar nebula by Turner et al. (2006). However, MRI effects are limited to the disk's surfaces and inner regions (inside ~ 1 AU) by the need for appreciable fractional ionization (Stone et al. 2000). The midplanes of protoplanetary disks are essentially unionized in the planet-forming regions from ~ 1 to ~ 15 AU, preventing MRI from serving as a driver of midplane disk evolution in these regions (Matsumura & Pudritz 2006). One is thus left with the gravitational torques in a marginally gravitationally unstable disk in order to drive global angular momentum transport. Such torques are quite effective in driving disk evolution on timescales as short as $\sim 10^5$ yrs (Boss 1998), while at the same time transporting tracers both far upstream and downstream (Boss 2004a). The latter models thus provide strong support for the situation envisioned by Prinn (1990): $k \gg 1$, because gravitational torques and convective motions are able to transport tracers far upstream, even in the absence of viscous evolution of the disk ($\nu = 0$) and of additional diffusive transport of the tracers ($D \approx 0$). The present models continue in this promising vein of investigation.

4. Initial Conditions

The models consist of a $1M_\odot$ central protostar surrounded by a protoplanetary disk with a mass of $0.091 M_\odot$ between 4 and 20 AU, as in Boss (2004a, 2006). Disks with similar masses appear to be necessary to form gas giant planets by core accretion (e.g., Inaba et al. 2003) or by disk instability (e.g., Boss et al. 2002). The disks start with an outer disk temperature $T_o = 50$ K, leading to a minimum in the Toomre Q value of 1.5 from ~ 8 to ~ 20 AU; inside 8 AU, Q rises to a value of ~ 9 because of the much higher disk temperatures closer to the protosun. A Q value of 1.5 implies marginal instability to the growth of gravitationally-driven perturbations, while $Q \sim 9$ implies a high degree of stability.

A color field representing SLRI or oxygen anomalies is sprayed onto the outer surface of an already evolving disk at a radial distance of either 6 or 15 AU, into a 90 degree (in the azimuthal direction) sector of a ring of width 1 AU, simulating the arrival of a R-T finger. The models include the effects of the diffusion of the color field with respect to the gaseous disk (described above) by a generic turbulent viscosity characterized by alpha disk parameters of $\alpha = 0, 0.0001$, or 0.01 . The low α value (0.0001) is small enough to have only a minor effect on the color field (Boss 2004a). For $\alpha \leq 0.0001$, the color field is transported and mixed primarily by a combination of the global actions of gravitational torques in the marginally gravitationally unstable disks and the local actions of convective-like motions (Boss 2004b).

SLRI or oxygen anomalies that reside in the gas or in particles with sizes of mm to cm

or smaller will remain tied to the gas over timescales of ~ 1000 yrs or so, because the relative motions caused by gas drag result in differential migration by distances of less than 0.1 AU in 1000 yrs, which is negligible compared to the distances they are transported by the gas in that time, justifying their representation by the color field. In addition, solids in a disk with spiral arms will not migrate monotonically toward the protosun to be lost to melting (Cuzzi & Zahnle 2004), but rather will be driven by gas drag forces to the centers of the spiral arms, where they can survive indefinitely (Haghighipour & Boss 2003a,b).

5. Results

We present here the results of six models, representing injection of the color field onto the disk surface at distances of either 6 AU or 15 AU, for three values of the eddy diffusivity of the color field with respect to the gas, quantified by $\alpha = 0.01$ (H), 0.0001 (L), or 0.0 (Z), for models 6H or 15H, 6L or 15L, and 6Z or 15Z, respectively.

The color fields shown in the figures represent the number density of small solids (e.g., chondrules, CAIs, ice grains, or their precursor grain aggregates) in the disk carrying either SLRI or oxygen isotope anomalies. In all the models, injection occurs after the disk has been evolving for a time of 200 yr, sufficient time for a marginally gravitationally unstable disk to develop a strongly non-axisymmetric pattern of spiral arms and clumps (Boss 2004a). In all the models, downward (and upward) transport occurs on short timescales (~ 30 yr) as a result of convective-like motions driven by the superadiabatic vertical temperature gradients between the disk's midplane and its upper layers that develop as the disk evolves and forms dense spiral arms and clumps in the midplane (Boss 2004b).

5.1. Inner Disk Injection

Model 6L involves a low level of color field diffusivity and injection at 6 AU. Fig. 1 shows that the color field initially sprayed onto the disk's surface at a distance of 6 AU is transported down to the midplane of the disk in less than 30 yr. Once the color field reaches the midplane, the effect of the gravitationally driven disk evolution is to transport the color field inward to 4 AU as well as outward to the disk boundary at 20 AU in less than 1000 yr (Fig. 2). For the next several 1000 yr, the color field continues to circulate around the disk and to mix with the disk gas (Fig. 3). Note that the color field piles up artificially on the inner and outer boundaries of the grid (Fig. 3); in a more realistic calculation, these color fields would disappear from the numerical grid, as the color was transported closer to the

central protostar and to the portions of the disk lying beyond 20 AU.

Model 6Z, with no eddy diffusivity at all, was started from model 6L at a time of 2506 yr. After almost another 1000 yr of evolution with $\alpha = 0$, Fig. 4 shows that model 6Z has evolved in very much the same manner as model 6L (cf., Fig. 3) at the same time. This shows that in model 6L, the effects of nonzero diffusivity are quite small in comparison to the mixing and transport that is accomplished by the gravitational torques and convective-like motions in the marginally gravitationally unstable disk.

The color fields shown in Figs. 3 and 4 represent the number density of SLRIs in disks after ~ 3283 yrs of evolution following the injection event. Given the strong gradients in the color fields evident in Figs. 3 and 4, it is clear that the color field is highly spatially heterogeneous. The underlying gas density distribution is equally highly non-axisymmetric, of course, and it is the gas density that drives the transport of the color field. What is really important to understand is the extent to which the color field has become homogeneous with respect to the disk gas. This is because cosmochemical SLRI abundances typically are given as ratios, i.e., $^{26}\text{Al}/^{27}\text{Al}$, where the SLRI ^{26}Al is derived from the injection event, whereas the reference stable isotope ^{27}Al is presumably derived primarily from a well-mixed presolar cloud. Hence in order to determine the variations in the SLRI ratio $^{26}\text{Al}/^{27}\text{Al}$, the color field must be normalized by the gas density. This has been done in Fig. 5, which shows the log of the color/gas ratio for model 6L at the same time as the color field in Fig. 3. It can be seen that the color/gas ratio is remarkably uniform throughout the disk, with variations of no more than 0.1 in the log, or no more than a factor of 1.26. The only exceptions to this uniformity are regions close to the inner and outer boundary where there is very little color and even less gas density, so that the ratio becomes large. Because these regions contain essentially no gas or color, these ratio variations are negligible. For comparison, Fig. 6 shows the color/gas ratio for model 6L at the same time as Fig. 1, soon after the color field has reached the midplane and before it has had time to mix with the gas: at this time the color/gas ratio field is strongly non-uniform wherever there is color. Within a few 1000 yr, this strong initial heterogeneity is largely erased by disk mixing and transport.

5.2. Outer Disk Injection

While both the inner and outer disk injection models are appropriate for considering SLRIs injected by R-T fingers, the outer disk injection models are considerably more appropriate for the mixing and transport of oxygen isotope anomalies than the 6 AU models, because such anomalies are most likely to survive only when formed at the disk surface at distances of 15 AU and beyond (Lyons & Young 2005).

Fig. 7 shows model 15L at about the same time as model 6L in Fig. 2, about 550 yr after the injection event. The color field has been transported throughout more of the disk than in model 6L at this time, as in model 15L the color field is able flow rapidly downstream toward the protostar, whereas in model 6L, the color field must fight its way upstream against this flow, and hence the large-scale transport is slower than in model 15L. The previous models (Boss 2004a), where injection incurred at 9 AU, display color field evolutions intermediate between those of the models with injection at 6 and 15 AU, as expected.

Fig. 8 shows the color/gas density ratio in the midplane of model 15L after 3491 yr, about the same time as that for model 6L, shown in Fig. 5. Once again the color/gas ratio has been transformed from a highly spatially heterogeneous distribution into a more nearly uniform distribution, with the exception of very low density regions close to the inner and outer boundaries.

5.3. Evolution of the Dispersion

While Figs. 5 and 8 demonstrate the approach to spatial homogeneity in these models, a more valuable quantity to calculate is the dispersion of the color/gas density ratio from its mean value, in order to make a more useful comparison with distributions of isotopic measurements.

Figs. 9 and 10 show the expected level of spatial heterogeneity in SLRI ratios such as $^{26}\text{Al}/^{27}\text{Al}$ as a function of time in the solar nebula, following a single SLRI injection event, for models 6L and 15L, respectively. The figures give the square root of the sum of the squares of the color field divided by the gas density subtracted from the mean value of the color field divided by the gas density, where the sum is taken over the midplane grid points and is normalized by the number of grid points being summed over. The sum excludes the regions close to the inner and outer boundaries, as well as regions with disk gas densities less than $10^{-12} \text{ g cm}^{-3}$, as the low gas densities in these regions skew the calculations of the dispersion of the ratio of color to disk gas, and these regions contain comparatively little gas and dust.

Figs. 9 and 10 show the evolution of the dispersion (or standard deviation) of the SLRI ratio from the mean value. The injection transient dies away on a timescale of ~ 1000 yrs, as expected, and in both models seems to reach a steady state dispersion level of $\sim 10\%$. This steady state value is more clearly reached in model 15L than in 6L, because of the longer time span covered by model 15L and because the colors are transported primarily downstream in model 15L, allowing a faster approach to a steady state, as is clear from comparing Figs. 9

and 10. By way of comparison, at the moment of injection, the ratio of color to gas density was highly spatially heterogeneous, being equal to zero everywhere except at the surface of the disk in an azimuthal sector at a distance from the protosun of between 5.5 and 6.5 AU in model 6L or between 14.5 and 15.5 AU in model 15L.

In order to determine if the $\sim 10\%$ level of dispersion is caused by the choice of the eddy diffusivity D , models 6L and 15L were continued with the eddy diffusivity turned off, i.e., $D = 0$, resulting in models 6Z and 15Z. If $D \neq 0$ is the cause of the 10% dispersion, then the apparent level of dispersion should change once the eddy diffusivity is turned off. Figs. 9 and 10 also show that even without any diffusion of the color field with respect to the gas, the dispersion still appears to hover at a value around 10%, instead of approaching zero, as might have been expected. These figures show that with $\alpha = 0.0001$, the effects of diffusivity are minimal. However, in models 6H and 15H, with $\alpha = 0.01$, the high diffusivity leads to a high dispersion (\sim unity), which does not appear to be compatible with the isotopic evidence for some degree of homogeneity in the nebula, and hence these models are not considered further here.

The results for models 6Z and 15Z imply that gravitational mixing is not 100% efficient – it is unable to completely homogenize an initial spatial heterogeneity. This is probably because gravity is a long-range force, able only to drive mixing over length scales where significant gravitational forces occur. In the case of these disk models, this corresponds to length scales comparable to the spiral arms and clumps that develop, which tend to have minimum length scales of no less than an AU or so, whereas the radial extent of a single grid cell is 0.16 AU. Even the convective-like motions that accompany the gravitationally-driven large-scale motions do not appear to be able to homogenize the color field down to the level of individual grid cells, as these motions are themselves associated with the large-scale motions being driven by the gravitational torques, which leads to large-scale granularity at the 10% level.

Finally, it is important to note that this 10% level of spatial heterogeneity cannot be caused by the finite numerical viscosity of the hydrodynamics code, because this intrinsic viscosity affects both the gas density and the color field in exactly the same way (their evolution equations are identical when $\alpha = 0$), so that numerical viscosity cannot produce variations in the color field to gas density ratio.

6. Discussion

The trend toward a steady state dispersion value consistent with a low degree of spatial heterogeneity in these models implies that cosmochemical variations in inferred initial $^{26}\text{Al}/^{27}\text{Al}$ ratios must be due primarily to temporal heterogeneity, preserving the role of SLRIs as accurate chronometers for the solar nebula. While these models were originally intended to simulate the process of injection of SLRI onto the surface of the solar nebula, they are also roughly applicable to the situation regarding the stable oxygen isotope anomalies, thought to be created quasi-continuously at the disk surface at distances of ~ 30 AU (Lyons & Young 2005). In a marginally gravitationally unstable disk, the optically thin surface will be dynamically evolving with a highly rippled surface (Jang-Condell & Boss 2007). One might expect then that the right conditions for generation of the oxygen anomalies will be a spatially and temporally varying process, rather than a continuous process across the entire disk surface. If so, then these models of instantaneous injection onto limited regions of the disk surface should be applicable as well to the mixing and transport of oxygen anomalies produced by UV photodissociation.

Boss (2006) presented a scenario for the transport of ^{16}O -poor ice grains formed at the disk surface at 20 AU and beyond (Lyons & Young 2005) inward to ~ 2.5 AU on timescales of $\sim 10^3$, as indicated by the present models and by those of Boss (2004a). This would change the oxygen composition of the inner disk from being ^{16}O -rich to ^{16}O -poor. Krot et al. (2005a) and Zanda et al. (2006) suggested that the unaltered oxygen isotopic compositions of chondrules and refractory inclusions (RI) resulted from the RI forming first in an ^{16}O -rich gas, followed by chondrule formation after the nebular gas had evolved to a more ^{16}O -poor composition. The present models support this type of explanation for the oxygen isotope anomalies observed in different components of primitive meteorites.

The basic result that initially spatially heterogeneous distributions tend to become homogenized to the extent that the dispersion from the mean value hovers around $\sim 10\%$ appears to be the result of the physics of mixing and transport in a marginally gravitationally unstable disk, rather than a result of the statistics of sampling rare events, e.g., the Poisson statistics of radioactive isotope decays. In the case of Poisson statistics, if the average number of events recorded in a given time interval is N , then the standard deviation of the number of events is $N^{1/2}$, which when divided by the average number of events is equal to $1/N^{1/2}$. This quantity is equivalent to the dispersion defined in this paper, which tends toward a value $\sim 10\%$. If this value were the result of Poisson statistics, then, it would imply that $N \sim 100$. It is unclear what the appropriate choice should be for N , but one choice could be the number of grid cells sampled. Given that the number of computational cells in the disk midplane used to calculate the dispersion in the present models is $\sim 25,000$,

if one took $N = 25,000$, and tried to use Poisson statistics to predict a dispersion based on this sampling of the finite number of grid cells, the result would be $1/N^{1/2} \sim 0.006$, not 0.1. Hence Poisson statistics cannot explain this result. In this context it should be noted that radioactive decay of the SLRI are not included in the present calculations, as the evolutions cover times (< 0.004 Myr) that are much shorter than the half-lives of the SLRI (e.g., the half-life of ^{26}Al is 0.7 Myr).

7. Conclusions

Refractory inclusions such as the CAIs have $^{26}\text{Al}/^{27}\text{Al}$ ratios that scatter by about 10% around the mean value of $\sim 4.5 \times 10^{-5}$ (MacPherson et al. 1995). This level of scatter in $^{26}\text{Al}/^{27}\text{Al}$ ratios appears to be consistent with the 10% dispersion found here to follow from an apparently stable level of spatial heterogeneity in the nebula. Such a relatively low level of spatial heterogeneity implies that even larger variations in initial $^{26}\text{Al}/^{27}\text{Al}$ ratios must be due primarily to temporal heterogeneity, preserving the crucial role of SLRIs like $^{26}\text{Al}/^{27}\text{Al}$ as accurate chronometers for the solar nebula. This $\sim 10\%$ level of heterogeneity also appears to be consistent with the preservation of the stable oxygen isotope anomalies produced by self-shielding at the outer disk surface (Lyons & Young 2005), followed by transport downward to the midplane and inward to regions of the nebula where such anomalies could also have been created but perhaps not sustained because disk surface temperatures there were too high for stability of the water ice grains that carried the isotopic anomalies.

We have shown that the degree of spatial heterogeneity in the solar nebula required for the use of the $^{26}\text{Al}/^{27}\text{Al}$ chronometer and for the survival of the oxygen isotope anomalies is consistent with the expectations for the mixing and transport of initially highly spatially heterogeneous tracers in a marginally gravitationally unstable disk. Such a solar nebula appears to be required for the formation of gas giant planets, such as Jupiter and Saturn, by either the core accretion (Inaba et al. 2003) or disk instability (Boss et al. 2002) mechanisms. MRI is often thought to be the source of the turbulent viscosity that is assumed to drive disk evolution across large distances (e.g., Gail 2002, 2004; Ciesla & Cuzzi 2006), but the presence of magnetically dead zones limits the applicability of MRI-driven turbulence to magnetically live regions, such as the disk surfaces. Marginally gravitationally unstable disk models offer a means to self-consistently calculate the mixing and transport of tracers throughout the planet-forming region. This large-scale transport seems to be required to explain observations of thermally processed, crystalline silicates in comets and protoplanetary disks (Nuth, Rietmeijer, & Hill 2002; van Boekel et al. 2005; Honda et al. 2006; Nuth & Johnson 2006). Marginally gravitationally unstable disks have the added attraction

of providing a robust source of shock fronts capable of thermally processing solids into the chondrules and other components found in the most primitive meteorites (Desch & Connolly 2002; Boss & Durisen 2005).

I thank Francis Albarede, James Lyons, and Joseph A. Nuth III for discussions, the referee for helpful comments, and Sandy Keiser for cluster and workstation management. This research was supported in part by the NASA Planetary Geology and Geophysics Program under grant NNG05GH30G and by the NASA Origins of Solar Systems Program under grant NNG05GI10G, and is contributed in part to the NASA Astrobiology Institute under grant NCC2-1056. Calculations were performed on the Carnegie Alpha Cluster, which was supported in part by NSF MRI grant AST-9976645.

REFERENCES

Alexander, C. M. O'D. 2004, *Geochim. Cosmochim. Acta*, 68, 3943

Amelin, Y., Krot, A. N., Hutcheon, I. D. & Ulyanov, A. A. 2002, *Science*, 297, 1678

Andreasen, R. & Sharma, M. 2006, *Science*, 314, 806

Becker, H., & Walker, R. J. 2003, *Nature*, 425, 152

Bizarro, M., Baker, J. A. & Haack, H. 2004, *Nature*, 431, 275

Bizarro, M., et al. 2006, *Meteoritics Planet. Sci.*, 41, A21

Boss, A. P. 1998, *ApJ*, 503, 923

———. 2004a, *ApJ*, 616, 1265

———. 2004b, *ApJ*, 610, 456

———. 2006, *Meteoritics Planet. Sci.*, 41, 1695

Boss, A. P., & Durisen, R. H. 2005, *ApJ*, 621, L137

Boss, A. P., & Myhill, E. A. 1992, *ApJS*, 83, 311

Boss, A. P., Wetherill, G. W. & Haghjipour, N. 2002, *Icarus*, 156, 291

Ciesla, F. J. & Cuzzi, J. N. 2006, *Icarus*, 181, 178

Ciesla, F. J. & Hood, L. L. 2002, *Icarus*, 158, 281

Clayton, R. N. 1993, *AREPS*, 21, 115

———. 2002, *Nature*, 415, 860

Cuzzi, J. N. & Zahnle, K. J. 2004, *ApJ*, 614, 490

Dauphas, N., Marty, B., & Reisberg, L. 2002, *ApJ*, 565, 640

Desch, S. J. & Connolly, H. 2002, *Meteoritics Planet. Sci.*, 37, 183

Desch, S. J., & Ouellette, N. 2005, *LPSC XXXVI*, #1327.

Foster, P. N. & Boss, A. P. 1997, *ApJ*, 489, 346

Gail, H.-P. 2002, *A&A*, 390, 253

———. 2004, *A&A*, 413, 571

Gounelle, M. et al. 2006, *ApJ*, 640, 1163

Guan, Y. et al. 2006, *Meteoritics Planet. Sci.*, 41, 33

Haghishipour, N. & Boss, A. P. 2003a, *ApJ*, 583, 996

———. 2003b, *ApJ*, 598, 1301

Halliday, A. 2004, *Nature*, 431, 253

Honda, M. et al. 2006, *ApJ*, 646, 1024

Hsu, W., Huss, G. R., & Wasserburg, G. J. 2003, *Meteoritics Planet. Sci.*, 38, 35

Iida, A., Nakamoto, T., Susa, H. & Nakagawa, Y. 2001, *Icarus*, 153, 430

Inaba, S., Wetherill, G. W. & Ikoma, M. 2003, *Icarus*, 166, 46

Jang-Condell, H. & Boss, A. P. 2007, *ApJ*, submitted

Krot, A. N. et al. 2005a, *ApJ*, 622, 1333

Krot, A. N., Yurimoto, H., Hutcheon, I. D. & MacPherson, G. J. 2005b, *Nature*, 434, 998

Limongi, M. & Chieffi, A. 2006, *ApJ*, 647, 483

Lisse, C. M. et al. 2006, *Science*, 313, 635

Lyons, J. R. & Young, E. D. 2005, *Nature*, 435, 317

MacPherson, G. J., Davis, A. M. & Zinner, E. K. 1995, *Meteoritics*, 30, 365

Marcus, R. A. 2004, *J. Chem. Phys.*, 121, 8201

Matsumura, S. & Pudritz, R. E. 2006, *MNRAS*, 365, 572

Mostefaoui, S., Lugmair, G., & Hoppe, P. 2005, *ApJ*, 625, 271

Nuth, J. A. & Johnson, N. M. 2006, *Icarus*, 180, 243

Nuth, J. A., Rietmeijer, F. J. M. & Hill, H. G. M. 2002, *Meteoritics Planet. Sci.*, 37, 1579

Ouellette, N. & Desch, S. J. 2006, *LPSC XXXVII*, #2348.

Prinn, R. G. 1990, *ApJ*, 348, 725

Sahijpal, S. & Soni, P. 2006, Meteoritics Planet. Sci., 41, 953

Shu, F. H., et al. 2001, ApJ, 548, 1029

Simon, S. B., et al. 1998, Meteoritics Planet. Sci., 33, 411

Sugiura, N., Miyazaki, A. & Yin, Q.-Z. 2006, Earth Planets Space, 58, 1079

Stevenson, D. J. 1990, ApJ, 348, 730

Stone, J. M., Gammie, C. F., Balbus, S. A., & Hawley, J. F. 2000, in Protostars and Planets IV, ed. V. Mannings, A. P. Boss, & S. S. Russell (Tucson: Univ. Arizona Press), 589

Tachibana, S. et al. 2006, ApJ, 639, L87

Thrane, K., Bizarro, M. & Baker, J. A. 2006, ApJ, 646, L159

Turner, N. J., Willacy, K., Bryden, G. & Yorke, H. W. 2006, ApJ, 639, 1218

van Boekel, R. et al. 2005, A&A, 437, 189

Vanhala, H. A. T. & Boss, A. P. 2000, ApJ, 538, 911

———. 2002, ApJ, 575, 1144.

Willacy, K., Langer, W., Allen, M. & Bryden, G. 2006, ApJ, 644, 1202

Wood, J. A. 2004, Geochim. Cosmochim. Acta, 68, 4007

Yin, Q., Jacobsen, S. B., & Yamashita, K. 2002, Nature, 415, 881

Young, E. D., et al. 2005, Science, 308, 223

Yurimoto, H., & Kuramoto, K. 2004, Science, 305, 1763

Zanda, B. et al. 2006, Earth Planet. Sci. Let., 248, 650

CMAX= 0.8000 CONDIF= 0.0100 R= 0.30E+15

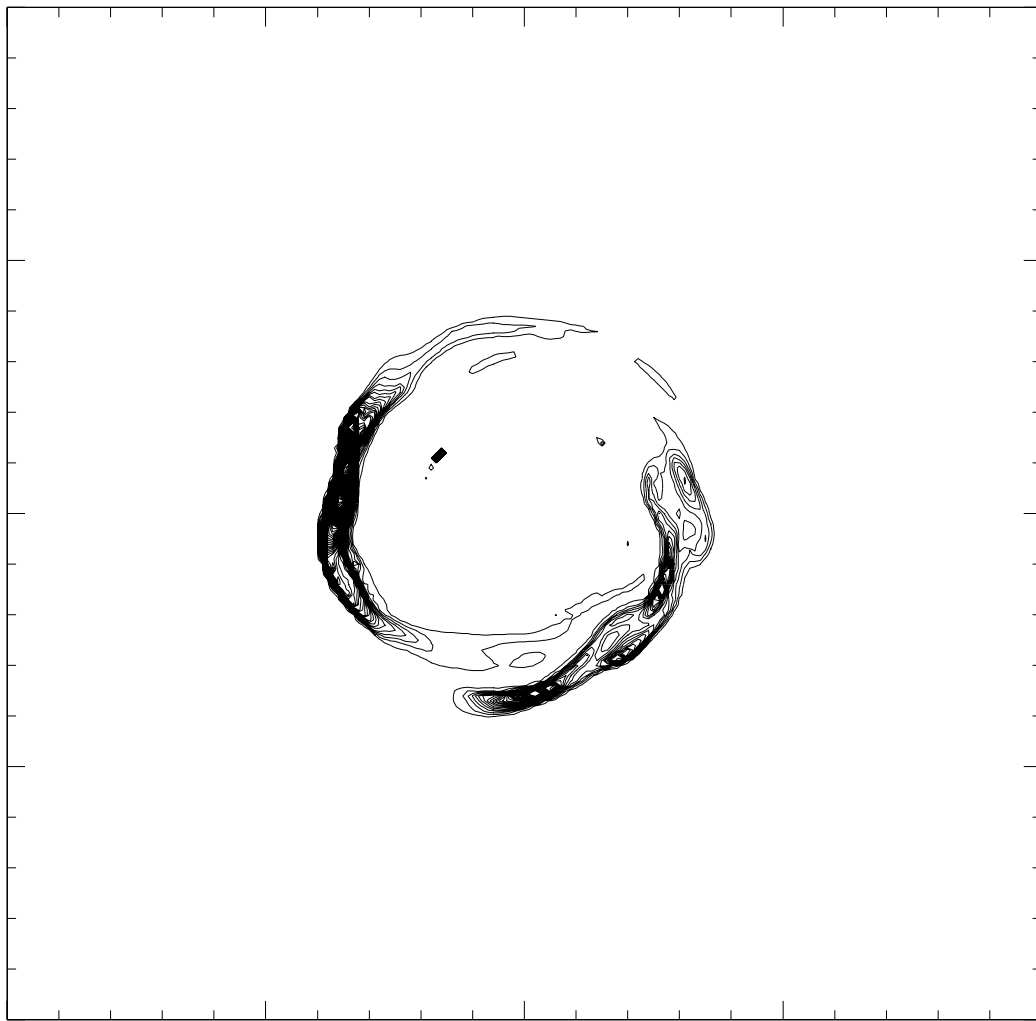


Fig. 1.— Model 6L at 227 yr, showing linear contours of the color field density (e.g., number of atoms of ^{26}Al cm^{-3}) in the disk midplane 27 yrs after the color field was sprayed onto the disk's surface in a 90 degree azimuthal sector between 5.5 and 6.5 AU. Region shown is 20 AU in radius (R) with a 4 AU radius inner boundary. In this Figure, the contours represent changes in the color field density by 0.01 units (CONDIF) on a scale normalized by the initial color field density of 1.0, up to a maximum value of 0.8 (CMAX). At this time, the color field has reached the midplane and begun to spread radially inward and outward.

CMAX= 0.1000 CONDIF= 0.0010 R= 0.30E+15

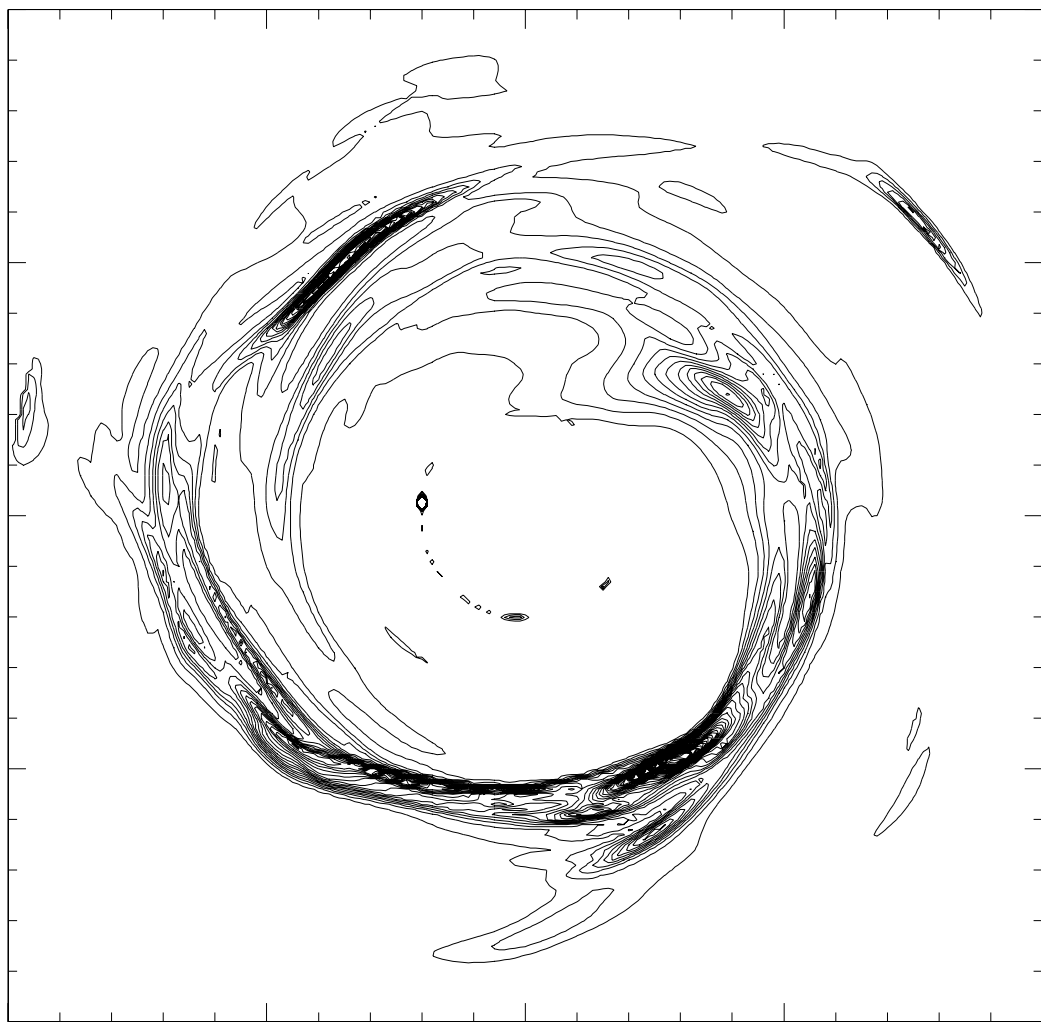


Fig. 2.— Same as Fig. 1, but after 760 yr. While the color field has spread throughout the radial extent of the disk, the spatial distribution is highly heterogeneous, with the highest concentrations residing inside the spiral arms of the disk.

CMAX= 0.0100 CONDIF= 0.0001 R= 0.30E+15

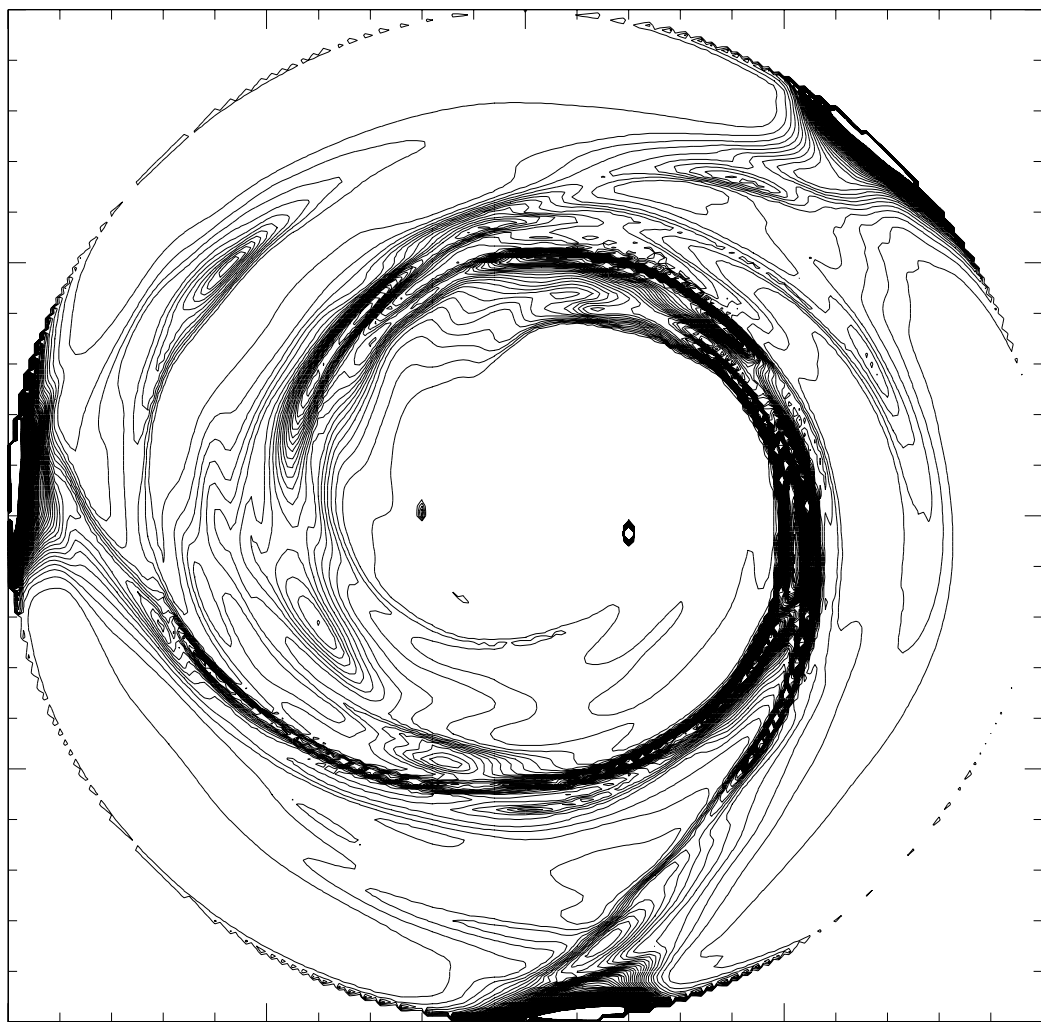


Fig. 3.— Same as Fig. 1, but after 3484 yr. The color clumps on the inner and outer boundaries are artifacts of the way the boundaries are handled.

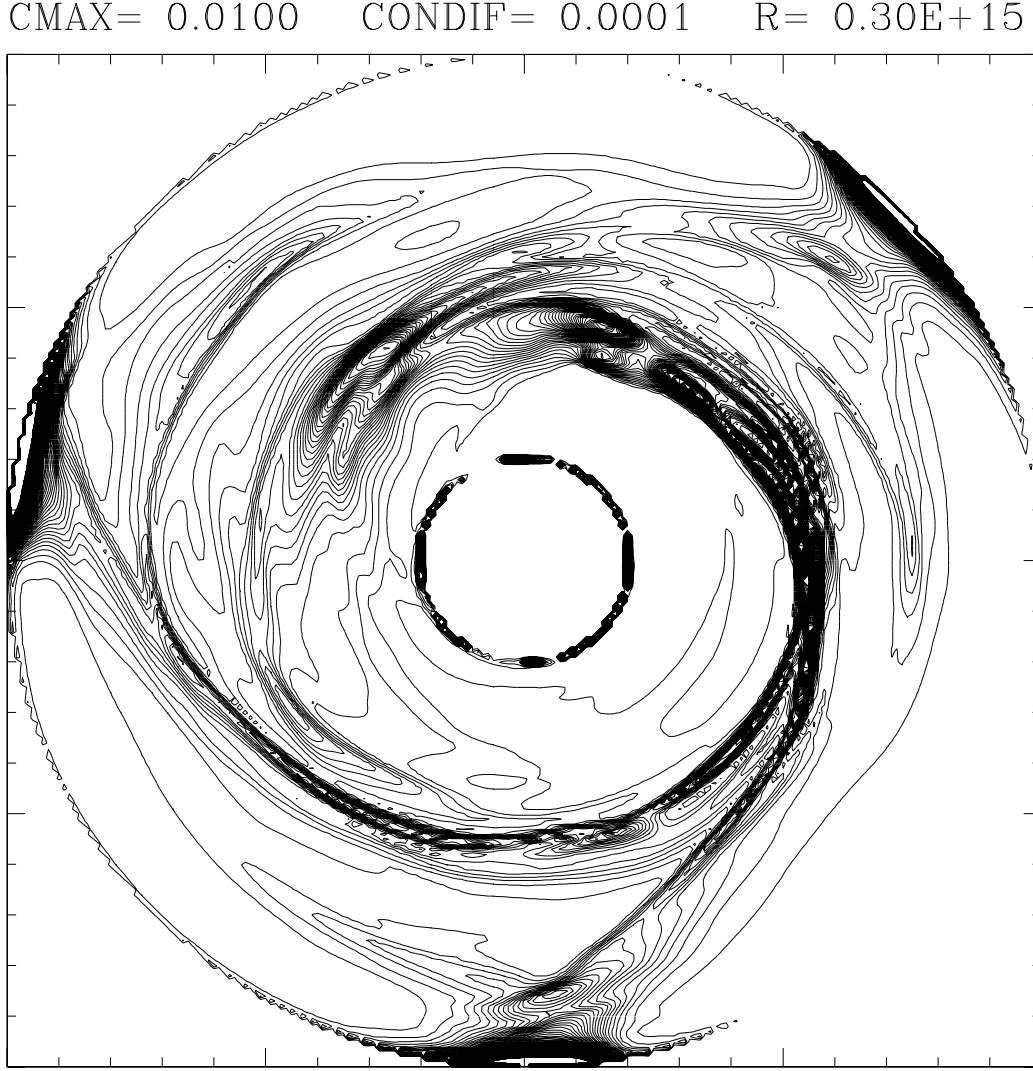


Fig. 5.— Logarithmic contours of the color field density divided by the disk gas density (i.e., log of the abundance ratio $^{26}\text{Al}/^{27}\text{Al}$) for model 6L at a time of 3484 yr, plotted in the same manner as in Fig. 1. Contours represent changes by factors of 1.26 up to a maximum value of 8.0; on a scale defined by the gas disk density. The abundances of SRI injected by a supernova are rapidly homogenized to within $\sim 25\%$, except for inside very low gas density regions adjoining the artificial inner and outer boundaries. [figure deleted to fit on astro-ph – can be seen in files on <http://www.dtm.ciw.edu/boss/ftp/nebulaviii>.]

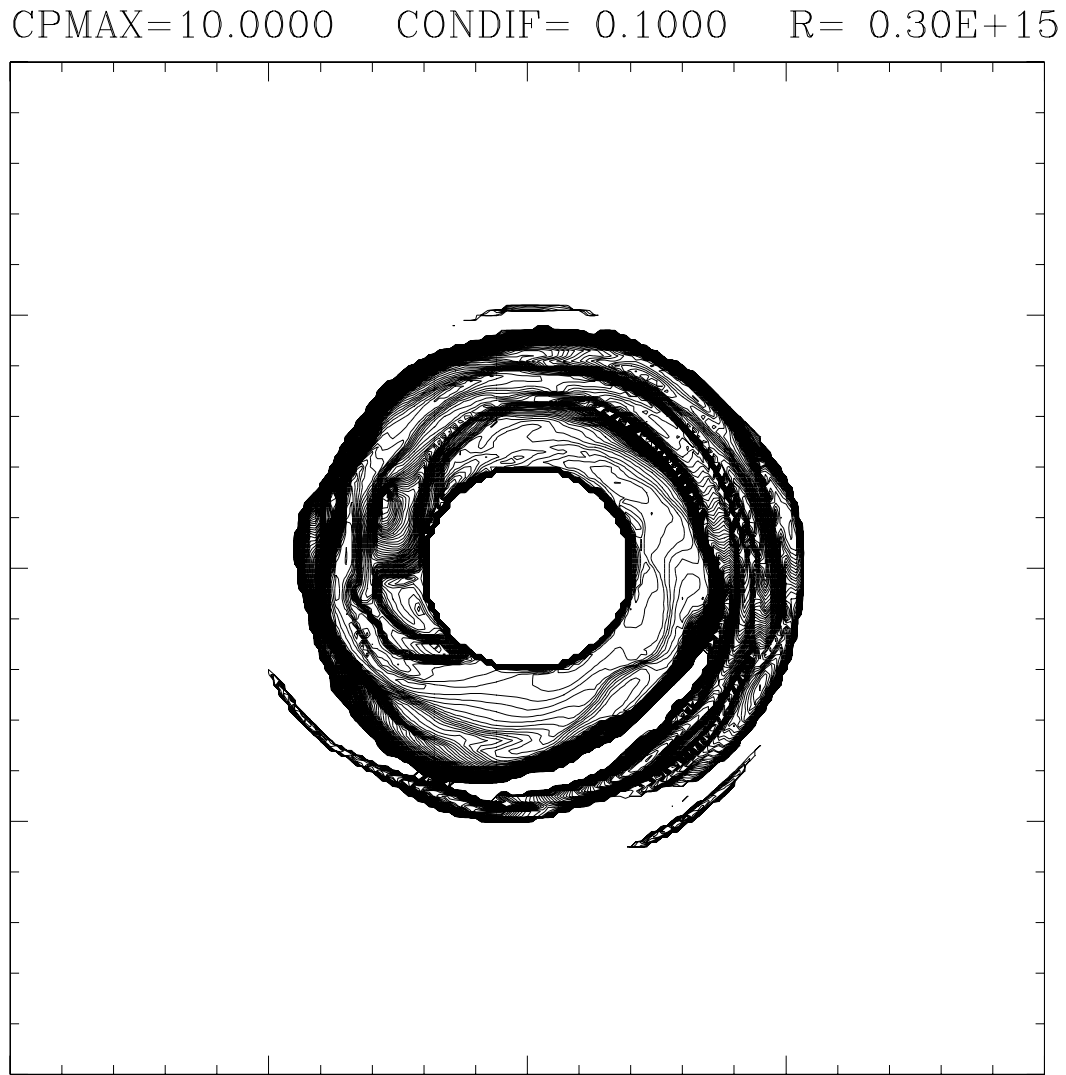


Fig. 6.— Same as Fig. 5 for model 6L, but at an earlier time of 227 yr (same time as Fig. 1). The color/gas density ratio is highly non-uniform at this early phase, before the marginally gravitationally unstable disk has had a chance to transport the color field radially inward and outward and to mix the field with the disk gas.

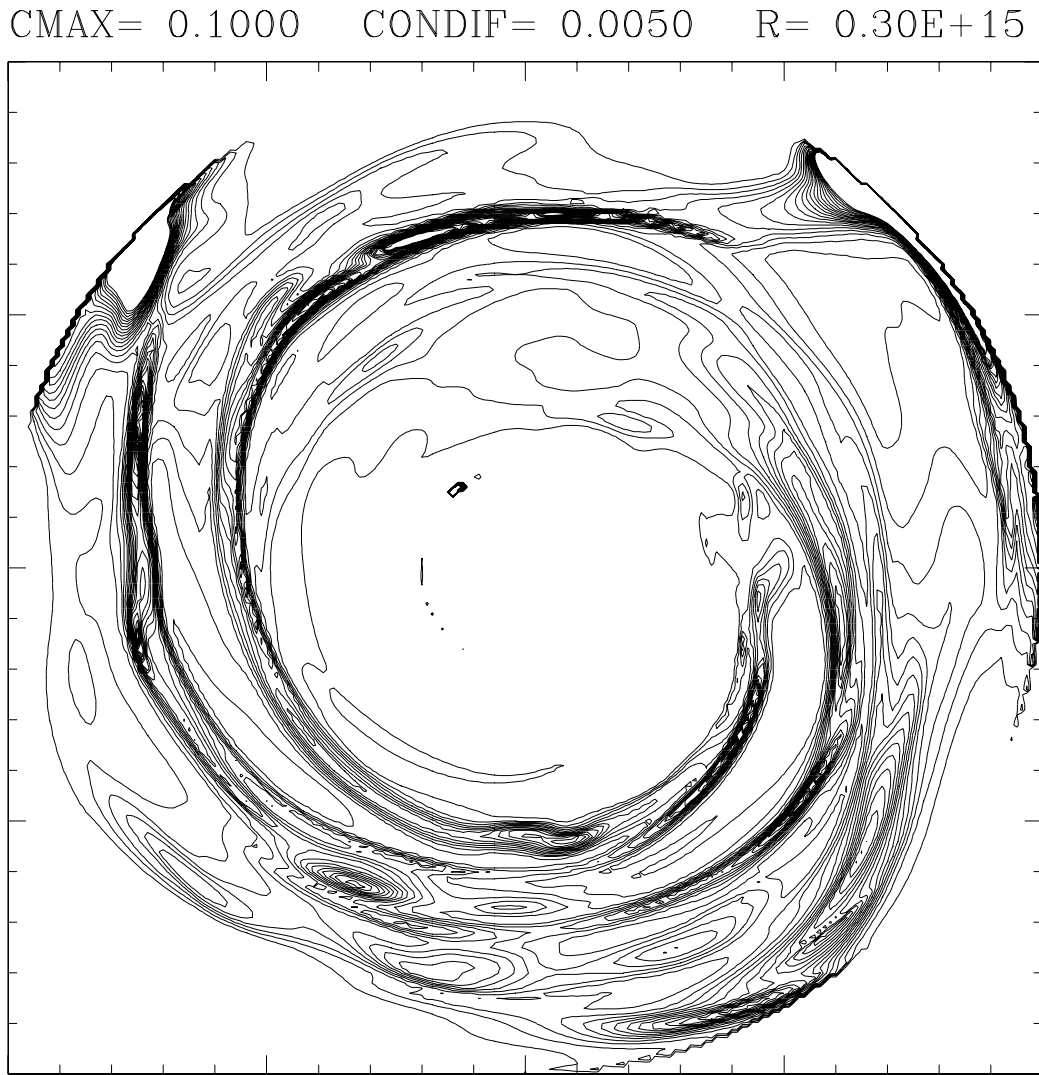


Fig. 8.— Same as Fig. 5, but for model 15L at a time of 3491 yr. Once again, the $\text{H}_2\text{O}/\text{gas}$ density ratio has become highly uniform as a result of mixing and transport, with the exception of the low-density regions at the boundaries. [figure deleted to fit on a page of 15 A4; instead see files on <http://www.dtm.ciw.edu/boss/ftp/nebulaviii/>.]

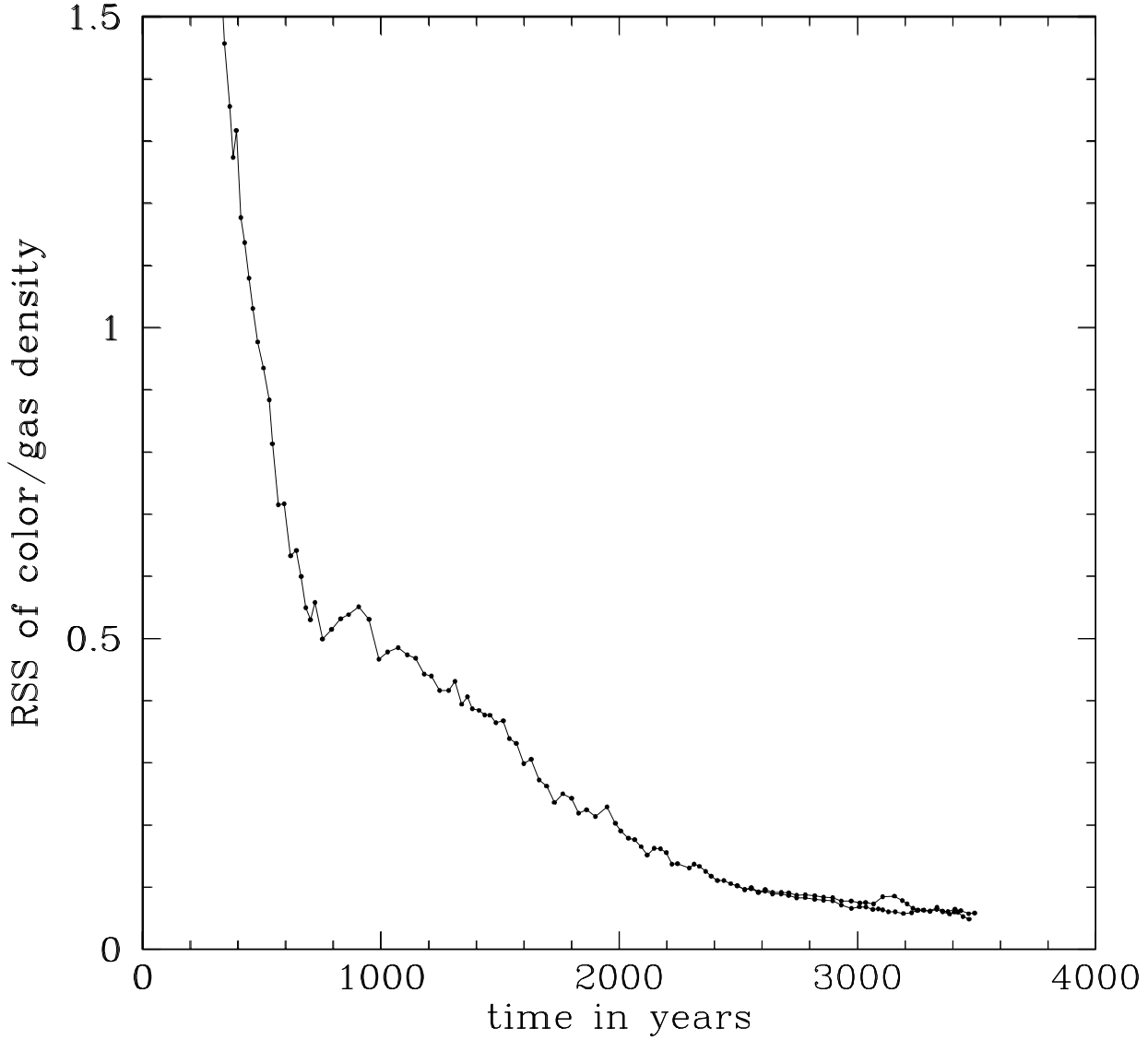


Fig. 9.— Time evolution of the dispersion from the mean (i.e., standard deviation, or the root of the sum of the squares [RSS] of the differences from the mean) of the color field density divided by the gas density (e.g., $^{26}\text{Al}/^{27}\text{Al}$ abundance ratio) in the disk midplane in model 6L. The color field is sprayed onto the disk surface at a time of 200 yrs. Starting from high values (RSS at 200 yrs is $\gg 1$), the dispersion decreases on a timescale of ~ 1000 yrs, then approaches a steady state value of $\sim 10\%$. After ~ 2600 yr, the results for model 6Z are plotted as well, resulting in the slightly lower sequence of values.

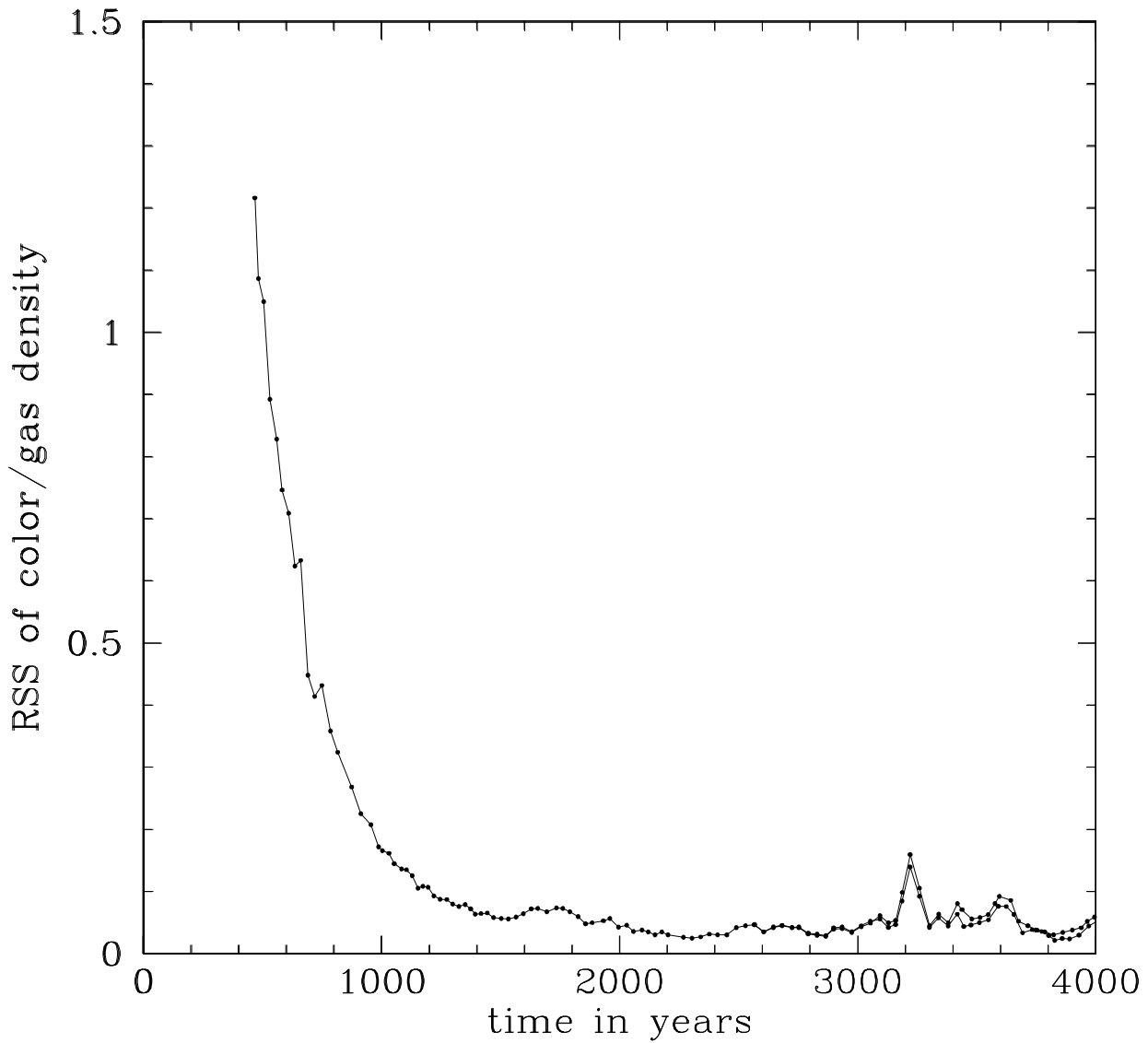


Fig. 10.— Same as Fig. 9, but for models 15L and 15Z, except that in this case the values for model 15Z are slightly higher than those for 15L.